Model Calculations and Interferometer Measurements of Ice-Cloud Characteristics

*SUNGGI CHUNG, STEVEN ACKERMAN, AND PAUL F. VAN DELST

Cooperative Institute for Meteorological Satellite Studies, University of Wisconsin—Madison, Madison, Wisconsin

W. PAUL MENZEL

National Oceanic and Atmospheric Administration National Environmental Satellite, Data, and Information Service Office of Research and Applications, Madison, Wisconsin

(Manuscript received 2 September 1998, in final form 24 May 1999)

ABSTRACT

This paper investigates the relationship between high–spectral resolution infrared (IR) radiances and the microphysical and macrophysical properties of cirrus clouds. Through use of radiosonde measurements of the atmospheric state at the Department of Energy's Atmospheric Radiation Measurement Program site, high–spectral resolution IR radiances are calculated by combining trace gas absorption optical depths from a line-by-line radiative transfer model with the discrete ordinate radiative transfer (DISORT) method. The sensitivity of the high–spectral resolution IR radiances to particle size, ice-water path, cloud-top location, cloud thickness, and multilayered cloud conditions is estimated in a multitude of calculations.

DISORT calculations and interferometer measurements of cirrus ice cloud between 700 and 1300 cm^{-1} are compared for three different situations. The measurements were made with the High–Spectral Resolution Interferometer Sounder mounted on a National Aeronautics and Space Administration ER-2 aircraft flying at 20-km altitude during the Subsonic Aircraft Contrail and Cloud Effects Special Study (SUCCESS).

1. Introduction

The importance of cirrus to the earth radiation budget has been established (Stephens and Webster 1981; Liou 1986). The global distributions of ice-water content and crystal size of cirrus are needed to improve the representation of cirrus in climate models. Such a characterization is expected to come by interpreting the satellite measurements of the infrared (IR) radiance. In the next several years, the Atmospheric Infrared Radiation Sounder on the Earth Observing System (EOS)-PM platform in 2002 and the Infrared Atmospheric Sounding Interferometer on the Meteorological Operational Platform (METOP) in 2003 will place high–spectral resolution infrared sounders into polar orbit. Also, the Moderate-Resolution Imaging Spectroradiometer will introduce high–spatial resolution global imaging in cirrus-sensitive spectral bands on *EOS-AM* (launched in 1999) and subsequently on EOS-PM. This paper investigates the extent to which these future remote sensing systems will be able to infer ice-particle size and ice-water paths of cirrus so that the effect of these clouds on the earth radiation budget will be understood more fully.

As a first step, an algorithm for retrieving cirrus properties has been developed based on the discrete ordinate radiative transfer (DISORT) method to build a reliable means of characterizing cirrus cloud from remote sensing. At this initial stage, the particles are treated as spheres and the scattering function is approximated by the Henyey–Greenstein function, although more realistic representations are becoming available (Stephens 1980; Takano et al. 1992). The computational procedure with spheres is simple and well established. For this reason, this set of calculations will serve a useful purpose for comparison when calculations are repeated with more realistic shapes. The retrieval performance of this algorithm is assessed by comparing with the High–Spectral Resolution Interferometer Sounder (HIS) measurements (Ackerman et al. 1990; Smith et al. 1993, 1998) because the atmospheric conditions and the cloud geometry are well known at the time of these HIS measurements. The cloud parameters are inferred by minimizing the difference between theoretical calculations and the interferometer observations in the wavenumber range of 700–1300 cm^{-1} by visual inspection. This process also is guided by the root-mean-square (rms) de-

* Deceased.

Corresponding author address: Dr. W. Paul Menzel, NOAA/NESDIS/ORA, 1225 W. Dayton St., Madison, WI 53706.
E-mail: paulm@ssec.wisc.edu

viation between the calculation and observation. The accuracy of the retrieved effective microphysical properties is tied fundamentally to accurate specification of the cloud boundaries. In the referenced studies, cloud boundaries were specified with lidar measurements. In the absence of a lidar, a single cloud effective altitude may be assigned using the carbon dioxide (CO_2) slicing method (Smith and Frey 1990).

A description of the DISORT model is presented in section 2. The sensitivity of high–spectral resolution IR observations to cirrus cloud microphysical and macrophysical properties with simulated datasets is investigated in section 3. Particle size and ice-water path are explored in sections 3a and 3b, respectively. Section 3c investigates the sensitivity of high–spectral resolution measurements to cloud property retrieval in the presence of errors in cloud boundary assignment. Simulations showing the errors associated with retrievals under multilayered cloud conditions are presented in section 3d. Section 3e describes simulations that assess the sensitivity of the high–spectral resolution measurements to vertical variations in cloud particle size.

Comparisons between HIS measurements and the current calculations, along with the retrieved effective particle size and ice-water path, are presented in section 4. Conclusions are made in section 5.

2. Calculation of emitted spectra for ice clouds

The differential equation for radiative transfer is well known (Chandrasekhar 1960; Stamnes et al. 1988; Tsay et al. 1990). Using the algorithm of Stamnes et al. (1988),

$$\mu \frac{du_\nu(\tau_\nu, \mu, \phi)}{d\tau} = u_\nu(\tau_\nu, \mu, \phi) - S_\nu(\tau_\nu, \mu, \phi), \quad (1)$$

where $u_\nu(\tau_\nu, \mu, \phi)$ is the (specific) intensity of monochromatic frequency ν in the plane-parallel layer of optical depth τ_ν in the direction of (μ, ϕ). Here ϕ is the azimuthal angle, and μ is the cosine of the zenith angle. The source function S_ν consists of

$$S_\nu(\tau_\nu, \mu, \phi) = \frac{\omega_\nu(\tau_\nu)}{4\pi} \int_0^{2\pi} d\phi' \int_{-1}^{1} d\mu' \times P_\nu(\tau_\nu, \mu, \phi; \mu', \phi') u_\nu(\tau_\nu, \mu', \phi') + Q_\nu(\tau_\nu, \mu, \phi), \quad (2)$$

where ω_ν is the single scattering albedo and $P_\nu(\tau_\nu, \mu, \phi; \mu', \phi')$ is the phase function. The first term on the right-hand side of the equation represents the multiple scattering. The second term represents the internal source and generally is written as

$$Q_\nu(\tau_\nu, \mu, \phi) = Q_\nu^{(\text{thermal})}(\tau_\nu, \mu, \phi) + Q_\nu^{(\text{beam})}(\tau_\nu, \mu, \phi), \quad (3)$$

$$Q_\nu^{(\text{thermal})}(\tau_\nu, \mu, \phi) = [1 - \omega_\nu(\tau_\nu)]B_\nu(T), \quad \text{and} \quad (4)$$

$$Q_\nu^{(\text{beam})}(\tau_\nu, \mu, \phi) = \frac{\omega_\nu(\tau_\nu)}{4\pi} I^{\text{inc}} P_\nu(\tau_\nu, \mu, \phi; -\mu_0, \phi_0) \times \exp(-\tau_\nu/\mu_0), \quad (5)$$

where $B_\nu(T)$ is the Planck function at temperature T, $Q_\nu^{(\text{beam})}$ arises from the usual distinction between direct and diffuse radiation, and I^{inc} and μ_0,ϕ_0 are the incident intensity and the solar angles, respectively.

In the DISORT method, the scattering phase function is expanded by the Legendre polynomials as

$$P(\tau_\nu, \cos\Theta) = \sum_{\ell=0}^{2N-1} (2\ell + 1) g_\ell(\tau_\nu) P_\ell(\cos\Theta), \quad (6)$$

where

$$\cos\Theta = \mu\mu' + [(1 - \mu^2)(1 - \mu'^2)\cos(\phi - \phi')]^{1/2}. \quad (7)$$

Accordingly, the intensity function is expanded as

$$u_\nu(\tau_\nu, \mu, \phi) = \sum_{m=0}^{2N-1} u_\nu^m(\tau_\nu, \mu) \cos[m(\phi_0 - \phi)]. \quad (8)$$

In this work, Eq. (1) is solved for one wavenumber at a time from 700.0 to 1300.0 cm^{-1} in steps of 0.1 cm^{-1} using the DISORT algorithm of Stamnes et al. 1988. The number of expansion terms $2N$ in Eqs. (6) and (8) is relevant to the accuracy of the numerical integration by Gaussian quadrature. Calculations with N equal to 16, 24, and 32 produce results within 0.02% of one another among the three sets in the entire range of 700–1300 cm^{-1}; as computer time was a minimal constraint, however, $N = 24$ (instead of $N = 16$) was adopted in this work. Contributions to the source function $Q_\nu^{(\text{beam})}$ in Eq. (3) from the sun are presumed to be insignificant in the infrared range between 700 and 1300 cm^{-1} and are ignored. The phase function is approximated by the Henyey–Greenstein function so that $g_\ell(\tau_\nu)$ in Eq. (6) is replaced by the ℓth power of the asymmetry factor, that is,

$$g_\ell(\tau_\nu) = g_{\text{asym}}^\ell(\tau_\nu). \quad (9)$$

The extinction coefficient (and hence τ_ν), the single-scattering albedo ω_ν, and the asymmetry factor $g_{\text{asym}}(\tau_\nu)$ are computed from Mie calculations for various clouds, assuming a Deirmendjian-type distribution function (Deirmendjian 1964) at radial distance r,

$$n(r) = ar^\alpha \exp(-br). \quad (10)$$

If the peak of the distribution function occurs at r_c, then

$$b = \alpha/r_c. \quad (11)$$

In this work, α is chosen to be 6. The normalization constant is given by

$$a = \left(\frac{\alpha}{r_c}\right)^{(\alpha+1)} \Big/ (\alpha!). \tag{12}$$

The ice particle is assumed to be spherical, and the particle size is measured in terms of the effective radius, defined as

$$r_{\text{eff}} = \frac{\int_0^\infty n(r) r^3 \, dr}{\int_0^\infty n(r) r^2 \, dr}. \tag{13}$$

The atmospheric temperature, pressure, and relative humidity as a function of the altitude are inferred from radiosondes launched from the Department of Energy Atmospheric Radiation Measurement (ARM) Program site (Lesht 1995). The clear-sky optical depths are computed as the integral sum of the absorption by water (H_2O) and other atmospheric molecules using a line-by-line radiative transfer model (LBLRTM) (Clough et al. 1992). The atmosphere (0.315–20.0 km) is divided into 56 layers so that the temperature difference across any boundary is no greater than 3.5 K. The theoretical calculations of spectra in ice-cloud situations are performed using the DISORT method (Stamnes et al. 1988).

3. Sensitivity studies

The particle effective size r_{eff} and the ice-water path (IWP) are important cirrus microphysical properties for radiative transfer. The cloud-top and -base altitudes also are important as they define the effective cloud temperature. This section examines how the cloud forcing is affected by these characteristic parameters. Cloud forcing is defined as the difference of upwelling radiance of the clear and cloudy skies, expressed as a brightness temperature. This difference is due solely to the presence of the cirrus cloud as an identical atmospheric condition is assumed in both cases. The shape of the cirrus ice crystals also is important in the IR region (Takano et al. 1992), but it is beyond the scope of this paper to examine the effect of shape.

a. Ice-particle size (r_{eff})

Variations in the cloud forcing spectra, resulting from the presence of a cirrus cloud, were investigated as a function of effective particle size r_{eff}. The DISORT calculation was performed for a 0.8-km-thick cloud layer at a cloud-top altitude of 10.8 km with an IWP of 10.0 g m^{-2}. Here and elsewhere, a layer of cloud is assumed to have a uniform r_{eff} and water density. Figure 1a shows the variation of the cloud forcing as a function of r_{eff}, ranging from 4.5 to 22.5 μm. In the IR window region between 800 and 900 cm^{-1}, the cloud forcing increases from 20 K for 22.5-μm ice particles to more than 65 K for 4.5-μm ice particles; the smaller particles cause more attenuation in the IR window radiation for a fixed IWP. The spectral change in cloud forcing from 800 to 1000 cm^{-1} shows a pronounced *S* shape for smaller ice particles (less than 10 μm), which becomes more linear for larger ice particles (greater than 10 μm). This *S* shape was reported previously by Smith et al. (1998) for 7.0-μm ice particles. This characteristic shape of the spectral cloud forcing between 800 and 1000 cm^{-1} for small and large ice particles is useful for distinguishing the ice-particle size ranges of cirrus clouds. Between 1100 and 1200 cm^{-1} the cloud forcing increases from about 15 to 40 K with decreasing ice-particle size, but there are no pronounced differences in the shape as r_{eff} is varied. In fact, in this range of wavenumbers, the cloud forcing is nearly constant as a function of wavenumber. Figure 1b is a companion plot to Fig. 1a in which the optical depth is kept constant (rather than the ice-water path). The variations of cloud forcing with the effective radius of ice particle are shown. The same general characteristics of Fig. 1a are apparent also in Fig. 1b.

Three radiative parameters are affected by a change of r_{eff}: the optical depth, albedo, and asymmetry factor. The cloud forcing between 800 and 1000 cm^{-1} is affected more by changes in τ than by changes in ω or g_{asym}. Thus, qualitatively speaking, the variation of r_{eff} manifests itself mainly through changes in τ between 800 and 1000 cm^{-1}. On the other hand, changes in all three parameters affect the region between 1100 and 1200 cm^{-1}.

b. Ice-water path and cloud opaqueness

The attenuation of radiation increases with increasing IWP and is wavenumber dependent. Figure 2 shows the spectral variation of the cloud forcing as IWP changes but r_{eff} is fixed at 7.5 μm. Cloud forcing at 1000 cm^{-1} increases from about 20 to 75 K as IWP increases from 7 to 80 g m^{-2}; the corresponding change at 800 cm^{-1} is 40–75 K. Large IWP renders the cloud opaque and the spectral cloud forcing becomes almost constant. The *S* shape of the cloud forcing is seen clearly for IWP equal to 7.0 and 15.0 g m^{-2} but is much less pronounced at IWP equal to 22.5–30.0 g m^{-2}. For IWP equal to 80.0 g m^{-2} the cloud forcing shows very little spectral dependence, and the cloud appears to be opaque. In this paper, a cloud is called opaque if the brightness temperature changes by less than 1 K across the spectrum as the underlying atmosphere changes with regard to temperature or humidity or the presence/absence of a lower layer of cloud. With this definition, clouds of r_{eff} equal to 7.5, 15.0, and 30.0 μm become opaque when the IWP exceeds about 45, 70, and 130 g m^{-2}, respectively.

c. Cloud altitude and thickness

Difficulties in defining the cloud altitude increase the uncertainty in the retrieved cloud properties. The cloud

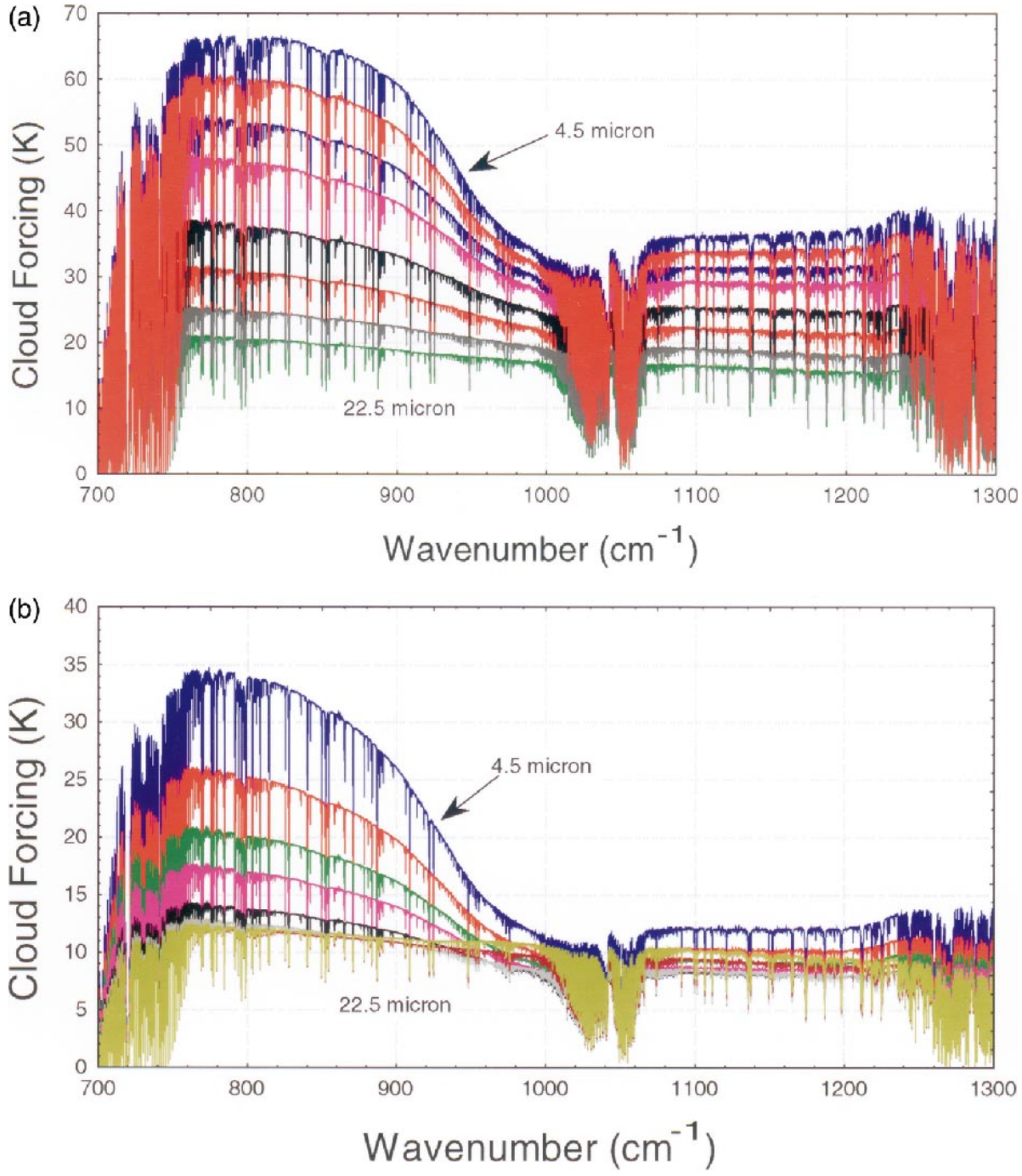

FIG. 1. The sensitivity of cloud forcing to the effective radius of cirrus cloud. Cloud forcing is defined as the brightness temperature difference between a clear- and a cloud-sky radiance. Eight different effective radii are assumed; they are (from the top curve to the bottom) 4.5, 6.0, 7.5, 9.0, 12.0, 15.0, 18.75, and 22.5 μm. In (a) the cloud has a constant IWP of 10 g m^{-2}, a cloud-top altitude of 10.8 km, and a thickness of 0.8 km. In (b) the cloud has a constant optical depth of 0.5 at 1000 cm^{-1}, a cloud-top altitude of 10.8 km, and a thickness of 0.8 km.

boundaries when measured by lidar contribute minimally to the overall error in the retrieved values. On the other hand, when CO_2 slicing is used, some uncertainty is expected. For example, in the cloud-top altitude measurements by CO_2 slicing, Frey et al. (1999) report an rms deviation of 500 m from lidar altitude. To estimate the impact of uncertainty in cloud-top altitude, a reference upwelling radiance was computed for a 1.1-km-thick cloud ($r_{\text{eff}} = 30$ μm and IWP = 20 g m^{-2}) at a cloud-top altitude of 11.1 km. The IWP was retrieved by minimizing the cloud-forcing difference between the reference and the calculated spectra in the 700–1300

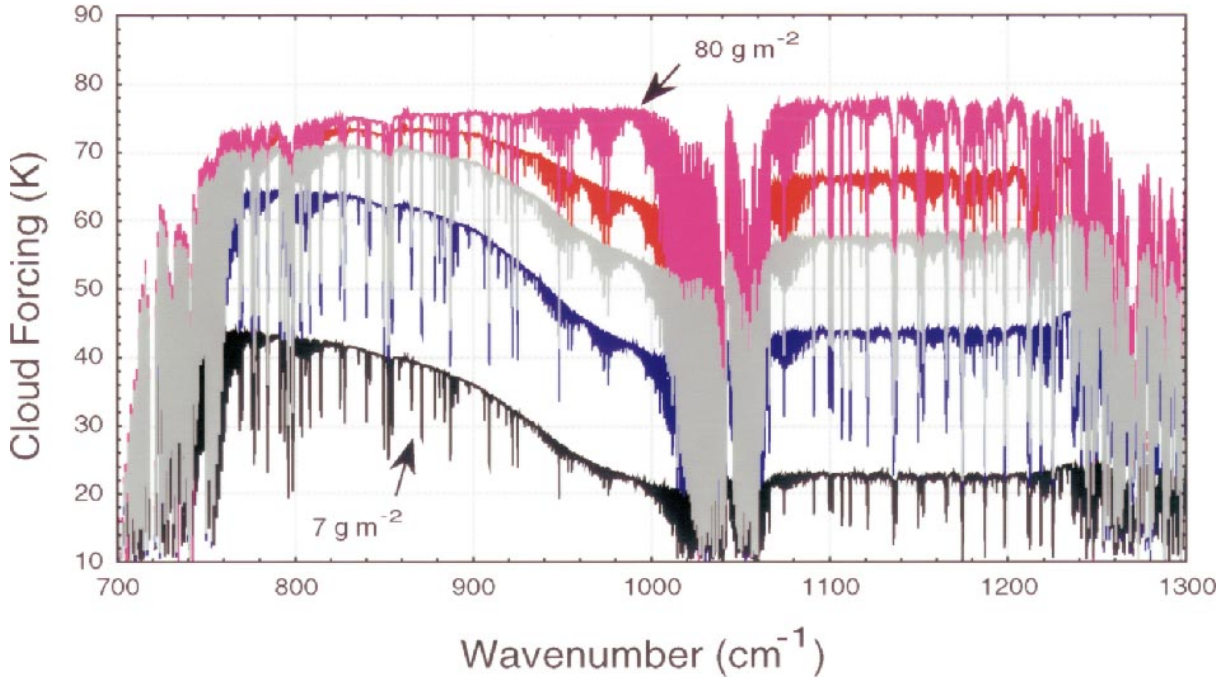

FIG. 2. Cloud forcing as a function of wavenumber for five different IWPs: 80, 30, 22.5, 15, and 7.0 g m^{-2} (from top to bottom). The clouds have the same r_{eff} of 7.5 μm, a cloud-top altitude of 10.8 km, and a thickness of 0.8 km.

cm^{-1} region. The IWP retrievals assumed a known clear-sky spectrum, cloud thickness of 1.1 km, and an r_{eff} of 30 μm. Figure 3 shows the error in the retrieved IWP as a function of the specified cloud-top altitude. An uncertainty of about 1.1 km in altitude leads to an IWP error of approximately 2 g m^{-2} (about 10%). As expected, assuming the cloud is too high results in a lower value for the retrieved IWP, and thus more radiance from below the cloud is transmitted to match the simulated observation. Assuming the cloud altitude is too low results in a retrieved IWP that is too large. The error is a nonlinear function with assumed cloud-top altitude; assuming the cloud is at 7.8 km increases the IWP error to 10 g m^{-2} (about 50%). This numerical experiment was continued with smaller effective radii. For a given wrong altitude, reproduction of the reference spectrum becomes increasingly difficult as r_{eff} is decreased, so that with r_{eff} equal to 7.5 μm and the wrong altitude of 9.0 km (in comparison with the 10.0-km reference), the best reproduction has deviations from the reference

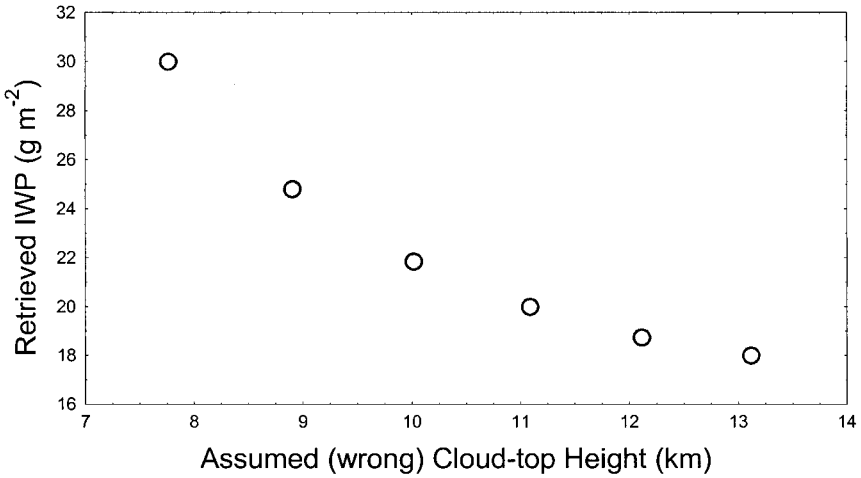

FIG. 3. Errors in retrieved IWP if the cloud-top altitude is assigned incorrectly during the retrieval. The ice cloud has an IWP of 20 g m^{-2}, an effective radius of 30 μm, and exists between 11.1 and 10.0 km.

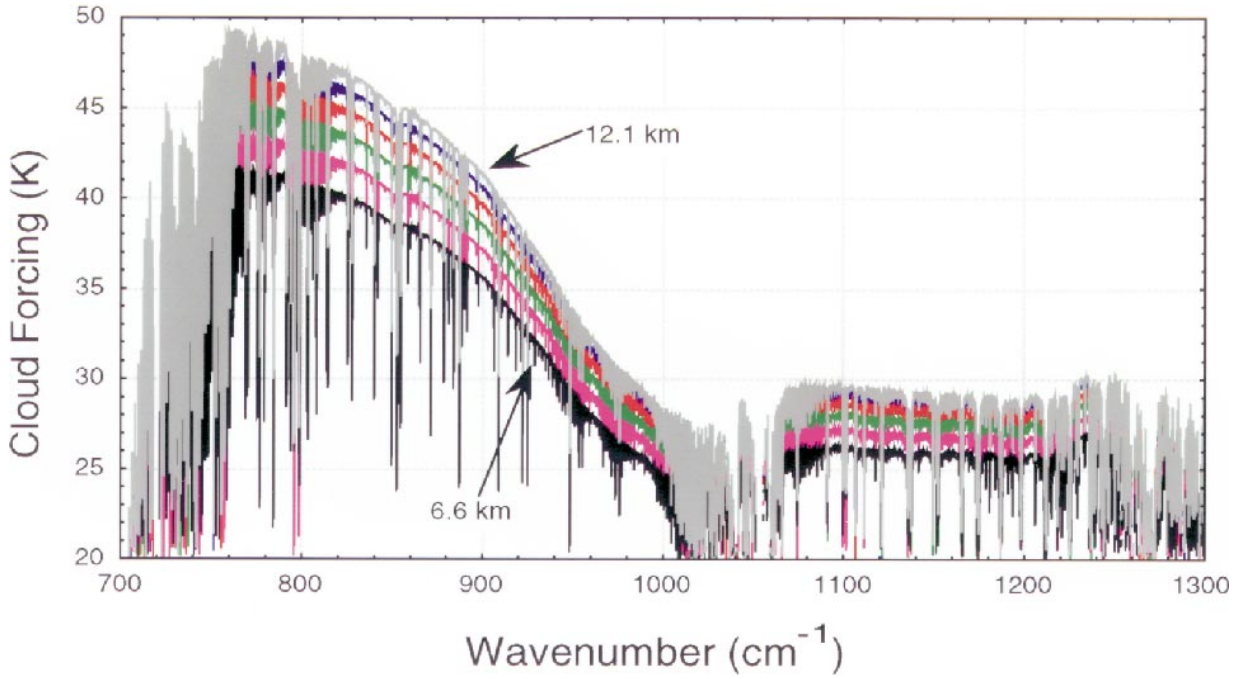

FIG. 4. Cloud forcing as a function of wavenumber for different cloud-base altitudes of 12.1, 11.1, 10.0, 8.9, and 7.8, and 6.6 km (from top to bottom). The cloud has a constant IWP of 10 g m^{-2} and an effective radius of 10.5 μm. The cloud-top altitude is 13.1 km.

spectrum of about $\pm$3 K. Thus, the sensitivity (error due) to the wrong altitude increases with smaller effective radii of cirrus cloud.

The sensitivity of the cloud-forcing spectrum with respect to the cloud thickness also was investigated. For a given cloud top (13.1 km) and IWP (10.0 g m^{-2}), the cloud-base altitude was varied from 12.1 to 6.6 km. Figure 4 shows the cloud-forcing spectrum as a function of the cloud-base (or cloud thickness). A 1-km error in cloud thickness leads to a decrease of cloud forcing of about 1.5 and 0.7 K in the wavenumber regions 800–1000 and 1100–1200 cm^{-1}, respectively. In comparison with the 5–50-K changes with particle size (see Fig. 1a), changes of 1.5 K or less indicate a relative insensitivity to the thickness of the cloud for fixed IWP.

d. Multilayered clouds

It is not unusual for a water cloud to exist below a cirrus cloud. To assess the IWP error caused by assuming a single-layered cirrus in a multilayered cloud condition, three sets of numerical experiments were undertaken. The upwelling radiances were computed for a cirrus layer (r_{eff} = 7.5 μm; IWP = 10, 20, or 40 g m^{-2}) at 11.1–10.0 km, with an underlying water cloud [r_{eff} = 20 μm; liquid water path (LWP) = 30 g m^{-2}] at the cloud-top altitudes ranging from 3.1 to 5.0 km with cloud thickness of approximately 1 km. In each case, IWP and r_{eff} were retrieved for an isolated cirrus cloud (the underlying water cloud is assumed to be undetected). The underlying cloud decreases the radiance at the cirrus cloud base and the retrieved cirrus IWP always is greater than the true value. Figure 5 shows the increase in the retrieved cirrus IWP as a function of the altitude of the unseen water cloud below. Not surprisingly, thin cirrus (IWP = 10 g m^{-2}) are more susceptible to changes in underlying conditions than are thick cirrus (IWP = 40 g m^{-2}); retrieved thin-cirrus IWP ranges from 14.5 to 19.5 g m^{-2} (with the retrieved r_{eff} between 9.6 and 10.875 μm), and thick-cirrus IWP ranges from 44 to 47 g m^{-2} (with the retrieved r_{eff} between 8.025 and 8.625 μm). The unseen water cloud at 5.0 km causes a greater change in the cirrus IWP than does the unseen water cloud at 3.1 km, because the emitting layer becomes colder with altitude.

e. Vertical variations in cloud-particle size

Most passive IR retrieval methods assume the cloud microphysics is distributed uniformly within the cloud. From several example replicator profiles introduced by Heymsfield (1999), there is the suggestion that a nominal midlatitude cirrus cloud can be thought of as having three layers. The upper 1 km consists of small 10- to 50-μm ice spheres, the next 1 km has large 300-μm columns, and the bottom 2 km reveal medium 150-μm aggregates, bullets, and rosettes. This section investigates the sensitivity of the high–spectral resolution radiances to the vertical distribution of particle size in the upper layers of a cirrus cloud with constant IWP. For these calculations, the cloud is divided into two layers; the upper layer occupies 11.1–10.0 km and the lower

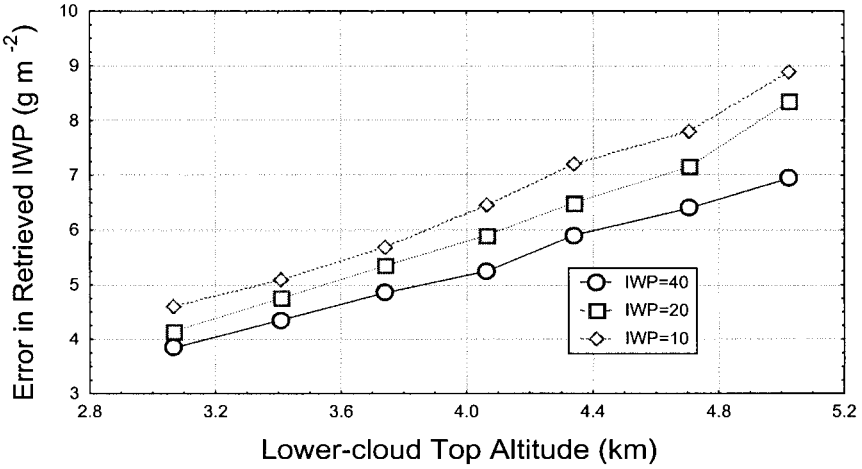

FIG. 5. Errors in retrieved IWP for a multilayered cloud condition, if a single 1-km-thick lower water-cloud layer is present but not accounted for. The cirrus cloud has an effective radius of 7.5 μm and exists between 11.1 and 10.0 km. The lower water cloud is approximately 1-km thick at altitudes ranging from 3.1 to 5.0 km and has an LWP of 30 g m^{-2} and an effective radius of 20 μm. The retrieved errors are shown for three cirrus IWP conditions: 40, 20, and 10 g m^{-2}.

layer goes from 10.0 to 8.9 km. One layer is composed of small particles (r_{eff} = 9.0 μm) and the other has large particles (r_{eff} = 22.5 μm); both layers have the same IWP (5 g m^{-2}). The cloud forcing of ''small particle over large'' and ''large particle over small'' is investigated. With the two layers placed at 10.0 and 11.1 km, calculations show that the cloud forcing by small over large is greater by 1–2 K than by large over small. Figure 6 shows the cloud forcing from these two cloud configurations; the net cloud forcing is similar to that of an ice cloud of particle size of about 13 μm. For this case study, it appears that the thin–cirrus cloud forcing is relatively insensitive to vertical variations in cloud particle size and is weighted toward the smaller particle size in average behavior.

4. Comparison with HIS measurements

This section presents comparisons of theoretical calculations of cirrus ice-cloud forcing and interferometer measurements between 700 and 1300 cm^{-1} for three different ice-cloud situations. The upwelling radiance spectra were observed by the HIS instrument mounted on a National Aeronautics and Space Administration (NASA) ER-2 aircraft flying at 20 km during the Subsonic Aircraft Contrail and Cloud Effects Special Study

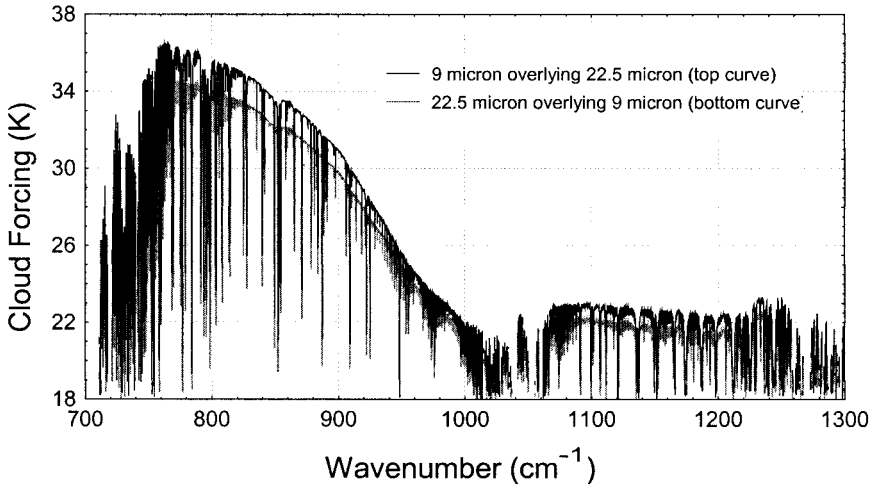

FIG. 6. The sensitivity of cloud forcing to variations in the vertical distribution of effective radius. Cloud forcing is defined as the brightness temperature difference between a clear-sky and a cloudy-sky radiance. In the top curve, the upper cloud layer has an effective radius of 9.0 μm and the lower layer has an effective radius of 22.5 μm. The particle sizes are reversed in the lower curve. The cloud has a constant IWP of 10 g m^{-2} and lies between 11.1 and 8.9 km.

(SUCCESS) on 21 April 1996 over the U.S. southern Great Plains. The HIS instrument is a Michelson interferometer with a spectral resolving power ($\lambda/\Delta\lambda$) of approximately 3000, covering the spectral range from 3.7 to 16.7 μm. The HIS spectra have an unapodized resolution of approximately 0.35 cm^{-1} from 600 to 1100 cm^{-1} and 0.7-cm^{-1} resolution from 1100 to 2700 cm^{-1}. Integrated high-emissivity, temperature-controlled reference blackbodies are used for an absolute calibration. The HIS instrument has a noise equivalent temperature and reproducibility of about 0.1–0.2 K over much of the spectrum. Revercomb et al. (1988) provide a detailed description of the instrument; Smith et al. (1998) report on the interferometer measurements from SUCCESS. Since the DISORT resolution (0.1 cm^{-1}) is different from that of HIS, for the purpose of comparisons, the former spectra are convoluted to the latter resolution using the HIS spectral response function.

Data from SUCCESS clouds labeled as 963, 990, and 998 (from 2024:50 UTC, 2029:20 UTC, and 2031:17 UTC, respectively, during the 21 April 1996 flight) were investigated. The HIS cloud forcing was determined using the observed spectra for cloudy and clear sky; the time between the measurements of the clear and cloudy skies is less than 20 min. DISORT calculations were performed using the radiosonde data from the ARM-site launch at 2030:00 UTC (the ARM site is within 150 km of the three clouds).

The DISORT calculation used the cloud (top and base) altitudes provided independently by the cloud and aerosol lidar system flying on the ER-2 aircraft (Spinhirne et al. 1996). Atmospheric temperature, pressure, and relative humidity were measured with the ARM-site radiosondes (Lesht 1995). These data were used to compute the optical depths from the atmospheric gases by using LBLRTM, which, in turn, become a part of the input data to DISORT. The extinction coefficient, single-scattering albedo, and asymmetry factor of the clouds are determined from the Mie calculations with the distribution function and the effective radius shown in Eqs. (10) and (13), respectively.

Retrieval of the effective radius and ice-water path was made by the following procedure. Numerous spectra were produced by DISORT from various combinations of r_{eff} and IWP, which are compared with the corresponding HIS spectra for a ''best'' reproduction of HIS spectra. Although a wide range of wavenumbers is used in comparison, no claim can be made that a unique r_{eff} and IWP can be retrieved. The rms deviations are considered in this retrieval process; they are based on spectral measurements and calculations at approximately 725 and 210 wavenumbers in the 800–1000 cm^{-1} and 1150–1200 cm^{-1} regions, respectively.

SUCCESS Cloud 998, observed at 2031:17 UTC on 21 April 1996, consists of two layers: one extends from 11.445 to 10.530 km (implying a thickness for the upper cloud of 0.915 km), and the other is found between 2.355 and 2.130 km (0.225-km thick). Here, two layers of Cloud 998 are assumed to have the same composition (i.e., same r_{eff}), so that the retrieved IWP represents the entire composite (two-layered) cloud. The r_{eff} and IWP are retrieved by matching the DISORT calculation to the HIS measurements, aided by rms calculations. Close agreement between the HIS measurement and DISORT calculation is found to occur with an r_{eff} in the range of 7.2–7.7 μm and with IWP in the range of 6.6–7.1 g m^{-2}. The rms differences of observed and calculated spectra are less than 1.5 K in 800–1000 cm^{-1} and 2.5 K in 1150–1250 cm^{-1}. Figure 7 shows the HIS spectrum and the DISORT calculation with r_{eff} of 7.35 μm and IWP equal to 6.85 g m^{-2}. To make it easier to distinguish the two spectra, 10 K is added to the HIS spectra in Fig. 7 (also in Figs. 8 and 9). The difference of the two spectra is shown as a third spectra near the bottom of the figure. The unusual inverted *S* shape in 800–1000 cm^{-1}, characteristic of small–particle size cirrus clouds, is apparent. As mentioned earlier, Smith et al. (1998) have reported an observation of this *S* shape and its association with small-particle cirrus. Their retrieved value of r_{eff} equal to 7.0 μm is in good agreement with the current calculation.

SUCCESS cloud 990, observed at 2029:20 UTC on 21 April 1996, is composed of layers at 10.515–9.690, 8.820–7.365, and 1.665–1.260 km. Again, a composite IWP for all three layers is retrieved. The best DISORT result is obtained with r_{eff} of 37.5 μm and IWP equal to 55.0 g m^{-2}; rms differences of observed and calculated spectra are 1.9 K (800–1000 cm^{-1}) and 4.1 K (1150–1250 cm^{-1}). Figure 8 shows the comparison between the HIS observation and the DISORT calculation. In contrast to the small-particle cirrus of Fig. 7, a larger-particle cirrus appears to be less sensitive to r_{eff} and IWP and the quality of the comparison does not change greatly as r_{eff} changes by 10.0 μm or IWP changes by 10 g m^{-2}. SUCCESS cloud 963, observed at 2024:50 UTC on 21 April 1996, has three layers from 10.830 to 9.600 km, 9.255 to 7.950 km, and 7.575 to 7.305 km. The current calculations suggest r_{eff} is 37.5 μm and the three-layer composite IWP is 604 g m^{-2}; rms differences are 1.8 K (800–1000 cm^{-1}) and 4.5 K (1150–1250 cm^{-1}). Both calculated and observed spectra of cloud forcing are shown in Fig. 9. The ground temperature was 295.2 K and the temperature at the top of the atmosphere (20 km) was 216.7 K so that the cloud forcing in excess of 70 K seen in Fig. 9 indicates that this cloud is almost completely opaque. In these large optical depths, the cloud forcing is insensitive to r_{eff} and IWP; therefore, the retrieved r_{eff} and IWP are subject to much greater uncertainty. No markedly different spectra are produced by changes of r_{eff} within 10.0 μm or IWP within 50 g m^{-2} for cloud 963. The cloud forcing spectra of clouds 990 and 963 in Figs. 8 and 9 also are nearly constant with wavenumber between 800 and 1000 cm^{-1} in contrast with cloud 998 in Fig. 7.

One may speculate that the assumption of spherical ice particles may be more forgiving in the smaller-par-

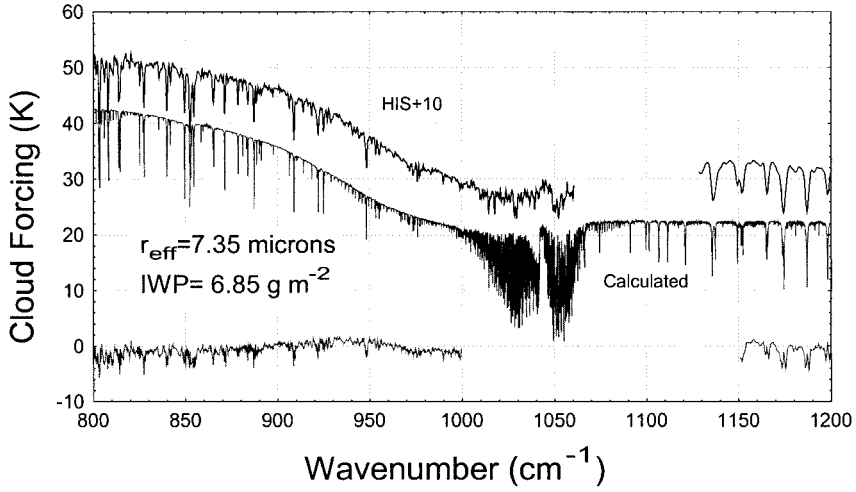

FIG. 7. Cloud forcing as a function of wavenumber for an HIS observed spectrum during the SUCCESS experiment (cloud 998) and results from a DISORT calculation with an effective radius of 7.35 μm and an IWP of 6.85 g m^{-2}. Here, 10 K is added to the HIS spectrum (top) for clearer distinction from the DISORT calculation (middle). The bottom spectrum is the difference between the two at wavenumbers of HIS resolution used in the rms calculation.

ticle case (cloud 998) than in larger-particle cases (cloud 990 or 963), because the comparison with HIS data is much better in cloud 998 than in the other cases. Further case studies are planned to explore this premise and to validate the use of Henyey–Greenstein functions.

5. Conclusions

Calculations of high–spectral resolution IR radiances in cirrus cloud situations indicate that cloud forcing (clear minus cloudy) spectra are sensitive to ice-particle size, ice-water path, and cloud altitude. They are less sensitive to cloud thickness and lower-layer clouds.

A numerical procedure based on the DISORT algorithm is used to retrieve the effective radius and ice-water path of cloud layers. The state of the atmosphere (temperature and H_2O profiles and optical depths of other atmospheric gases) is assumed to be known. The cloud boundaries in this work are determined by the airborne lidar system; alternatively, the CO_2-slicing method can be used with 500-m uncertainty (see section 3c). Ice particles were treated as spheres, and the scattering function was approximated by the Henyey–Greenstein function; future model calculations will incorporate more realistic particle shapes and scattering functions.

The best sets of effective radius and ice-water path can reproduce the observed HIS cloud forcing to within

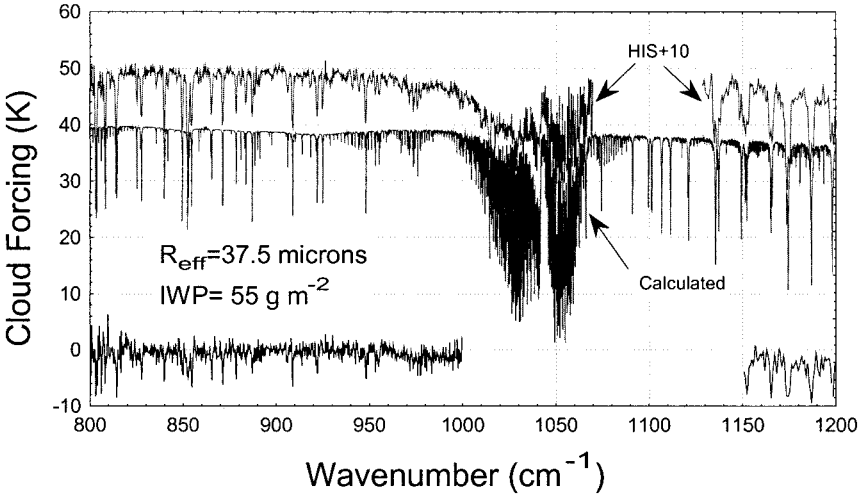

FIG. 8. Same as Fig. 7 but for cloud 990 and results from a DISORT calculation with an effective radius of 37.5 μm and an IWP of 55 g m^{-2}.

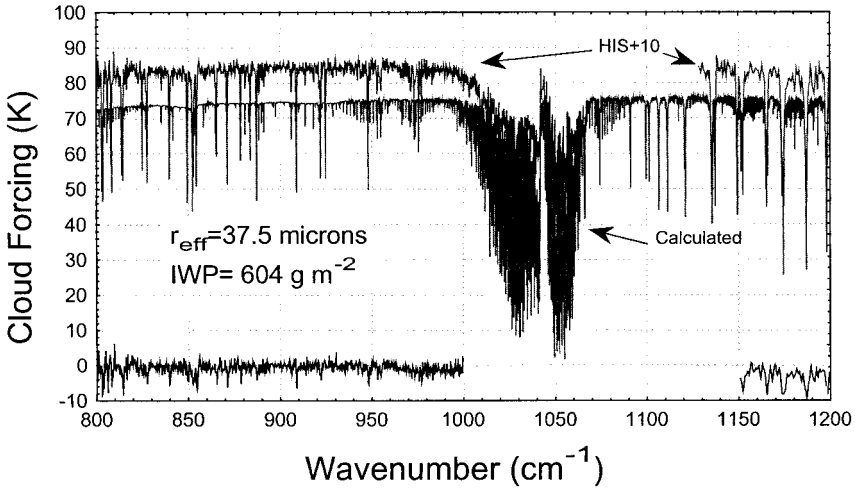

FIG. 9. Same as Fig. 7 but for cloud 963 and results from a DISORT calculation with an effective radius of 37.5 μm and an IWP of 604 g m^{-2}.

2 K in 800–1000 cm^{-1} and to within 4.5 K in 1150–1250 cm^{-1} for both small ($r_{\text{eff}} < 10$ μm)- and large ($r_{\text{eff}} > 10$ μm)-particle clouds. Measured HIS spectra have been used to infer a range of ice particle sizes between 7.5 and 37.5 μm with ice–water paths between 10 and 600 g m^{-2}. The reasonable reproduction in a wide window region shows the reliability of the DISORT-based algorithm. This process becomes less reliable, however, as the cloud opaqueness increases. Clouds with IWP greater than 50 g m^{-2} (130 g m^{-2}) and small (large) particles of r_{eff} of 7.5 μm ($r_{\text{eff}} = 30\mu$m) are found to be opaque (see section 3b).

One conclusion from these comparisons of measured and calculated spectra is that pending high–spectral resolution sounders in polar orbit on EOS and METOP will be capable of characterizing both r_{eff} and IWP with 20%–30% variation in the estimated values.

Another conclusion is that broadband (from 10 to 20 cm^{-1} resolution) measurements from the pending EOS imagers have the potential to distinguish large (>10 μm)– from small (<10 μm)–particle size cirrus clouds. It has been found that cirrus clouds with small ice particles exhibit a nonlinear *S*-shaped cloud forcing in 800–1000 cm^{-1} that gradually disappears as the particle size is increased. Utilizing this characteristic shape, three or four broadband measurements in the IR window region between 800 and 1000 cm^{-1} can be used for a rough distinction between the large– and small–particle size cirrus as well as IWP estimates. The spectra from 1000 to 1300 cm^{-1} do not show strong spectral dependence on r_{eff} and IWP; hence this spectral region may be useful for retrieving complementary optical depths. Suitable imager applications may include detection and mapping of the global distribution of aircraft contrails as well as cirrus clouds.

Acknowledgments. The authors gratefully acknowledge Drs. Wiscombe and Tsay for providing them with the computer code of DISORT. This work was funded by NASA Grant NAS5-31367.

REFERENCES

Ackerman, S. A., W. L. Smith, J. D. Spinhirne, and H. E. Revercomb, 1990: The 27–28 October 1986 FIRE IFO cirrus case study: Spectral properties of cirrus clouds in the 8–12 μm window. *Mon. Wea. Rev.*, **118,** 2377–2388.

Chandrasekhar, S., 1960: *Radiative Transfer*. Dover Press, 393 pp.

Clough, S. A., M. J. Iacono, and J.-L. Moncet, 1992: Line-by-line calculation of atmospheric fluxes and cooling rates: Application to water vapor. *J. Geophys. Res.*, **97,** 15 761–15 785.

Deirmendjian, D., 1964: Scattering and polarization properties of water clouds and hazes in the visible and infrared. *Appl. Opt.*, **3,** 187–196.

Frey, R. A., B. A. Baum, W. P. Menzel, S. A. Ackerman, C. C. Moeller, and J. D. Spinhirne, 1999: A comparison of cloud top heights computed from airborne lidar and MAS radiance data using CO_2 slicing. *J. Geophys. Res.*, **104,** 24 547–24 555.

Heymsfield, A., cited 1999: Vertical profiles of replicator data from two cases from FIRE-II (25 November and 5 December). [Available online at http://www.mmm.ucar.edu/science/cirrus/]

Lesht, B. M., 1995: An evaluation of ARM radiosonde operational performance. Preprints, *Ninth Symp. on Meteorological Observations and Instrumentation,* Charlotte, NC, Amer. Meteor. Soc., 6–10.

Liou, K. N., 1986: Influence of cirrus clouds on weather and climate processes: A global perspective. *Mon. Wea. Rev.*, **114,** 1167–1199.

Revercomb, H. E., H. Buijs, H. B. Howell, D. D. LaPorte, W. L. Smith, and L. A. Sromovsky, 1988: Radiometric calibration of IR Fourier transform spectrometers: Solution to a problem with the High Spectral Resolution Interferometer Sounder. *Appl. Opt.*, **27,** 3210–3218.

Smith, W. L., and R. Frey, 1990: On cloud altitude determinations from High Spectral Resolution Interferometer Sounder (HIS) observations. *J. Appl. Meteor.*, **29,** 658–662.

——, X. L. Ma, S. A. Ackerman, H. E. Revercomb, and R. O. Knu-

teson, 1993: Remote sensing cloud properties from high spectral resolution infrared observations. *J. Atmos. Sci.*, **50,** 1708–1720.

——, S. Ackerman, H. Revercomb, H. Huang, D. H. DeSlover, W. Feltz, L. Gumley, and A. Collard, 1998: Infrared spectral absorption of nearly invisible cirrus clouds. *Geophys. Res. Lett.*, **25,** 1137–1140.

Spinhirne, J. D., W. D. Hart, and D. Hlavka, 1996: Cirrus infrared parameters and shortwave reflectance relations from observations. *J. Atmos. Sci.*, **53,** 1438–1458.

Stamnes, K., S.-C. Tsay, W. Wiscombe, and K. Jayaweera, 1988: A numerically stable algorithm for discrete-ordinate-method radiative transfer in multiple scattering and emitting layered media. *Appl. Opt.*, **27,** 2502–2509.

Stephens, G. L., 1980: Radiative properties of cirrus clouds in the infrared region. *J. Atmos. Sci.*, **37,** 435–446.

——, and P. J. Webster, 1981: Clouds and climate: Sensitivity of simple systems. *J. Atmos. Sci.*, **38,** 235–247.

Takano, Y., K. N. Liou, and P. Minnis, 1992: The effects of small ice crystals on cirrus infrared radiative properties. *J. Atmos. Sci.*, **49,** 1487–1493.

Tsay, S.-C., K. Stamnes, and K. Jayaweera, 1990: Radiative transfer in stratified atmospheres: Development and verification of a unified model. *J. Quant. Spectrosc. Radiat. Transfer*, **43,** 133–148.